

Article

Reduction of Process Induced Porosity for Ultrafuse 316L through Parameter Optimization of Creality Ender 3 V2 and Makerbot Method X

Jeffery Logan Betts ^{1,2} , Bradley J. Sampson ^{1,2} , Kyle Lindsey ^{2,3}, Frank M. Brinkley ^{1,2} 
and Matthew W. Priddy ^{1,2,*} 

- ¹ Department of Mechanical Engineering, Mississippi State University, Mississippi State, MS 39762, USA; jlb1875@msstate.edu (J.L.B.); bs1875@msstate.edu (B.J.S.); fmb66@msstate.edu (F.M.B.)
² Center for Advanced Vehicular Systems, Mississippi State University, Starkville, MS 39759, USA; kl1430@msstate.edu
³ Department of Aerospace Engineering, Mississippi State University, Mississippi State, MS 39762, USA
* Correspondence: mwpriddy@me.msstate.edu

Abstract: Metal-based additive manufacturing (MBAM) has enabled rapid prototyping and one-off production, but the cost of equipment has limited widespread adoption. Recent developments in hybrid filaments and processes have created more accessible methods for MBAM, leveraging common fused filament fabrication (FFF) printers and Ultrafuse 316L metal filament. This technique has shown promise but suffered from large pore formations along parallel print paths. To reduce the formation of process-dependent pores, a design of experiments (DOE) was conducted to investigate the effects of varying extrusion parameters such as layer height, line width, and extrusion multiplier for tensile samples produced on a Creality Ender 3 V2 and MakerBot Method X. Characterization techniques included tensile testing, microhardness, density measurements, and optical microscopy; findings were compared to samples produced via laser-powder bed fusion (L-PBF) and from 316L plate. The Method X produced components with approximately 1% porosity and the Ender 4% porosity. Mechanical properties for both FFF printers were comparable to previous research, with an increase in tensile strength for the Method X. Despite the increased porosity in the Ender samples, only a 7% reduction in strength from the average yield in Method X samples (153.6 MPa) was observed. It was found that a combination of increased layer height and extrusion rate led to improved mechanical properties in parts printed on the Ender, while the default Makerbot settings resulted in the best overall performance for Ultrafuse 316L samples.

Keywords: additive manufacturing (AM); ultrafuse 316L; fused filament fabrication (FFF); laser-powder bed fusion (L-PBF); metal based additive manufacturing (MBAM); 316L stainless steel; material extrusion (MEX)



Citation: Betts, J.L.; Sampson, B.J.; Lindsey, K.; Brinkley, F.M.; Priddy, M.W. Reduction of Process Induced Porosity for Ultrafuse 316L through Parameter Optimization of Creality Ender 3 V2 and Makerbot Method X. *Crystals* **2024**, *14*, 285. <https://doi.org/10.3390/cryst14030285>

Academic Editor: Liqun Li

Received: 1 March 2024

Revised: 14 March 2024

Accepted: 15 March 2024

Published: 20 March 2024



Copyright: © 2024 by the authors. Licensee MDPI, Basel, Switzerland. This article is an open access article distributed under the terms and conditions of the Creative Commons Attribution (CC BY) license (<https://creativecommons.org/licenses/by/4.0/>).

1. Introduction

Additive Manufacturing (AM) has enabled the rapid manufacturing of prototypes, one-off productions, and complex geometries that traditional manufacturing could not achieve effectively. Fused filament fabrication (FFF) has undergone wide spread adoption, enabling printing of thermoplastics such as PLA and ABS [1]. Metal based additive manufacturing (MBAM) has enabled the use of additive manufacturing for structural components that require the durability and performance of metallic materials [2,3]. Many MBAM processes are well established, such as laser-powder bed fusion (L-PBF), which creates 3D geometries by melting metallic powder in an inert environment in a layer wise fashion [4–6]. While L-PBF can be enabling for unique geometries and alloys, the equipment, infrastructure, and associated hazards are complex and potentially cost prohibitive for smaller scale research/commercial efforts.

While FFF printing has been historically limited to thermoplastics, metal extrusion additive manufacturing (metal MEX) has enabled methods to create metallic components with FFF hardware and post-processing. Metal MEX originated by re-purposing FFF equipment and experimental methodologies before all-in-one commercial solutions from MarkForged and Desktop Metal came to market which are comparable in cost to some L-PBF machines. Instead, hybrid materials like Ultrafuse 316L (BASF 3D Printing Solutions GmbH, Heidelberg, Germany) metal filament can be utilized to create fully dense metallic components on common FFF printers, with post-processing standardized and outsourced [7]. Ultrafuse 316L metal filament is comprised of 316L stainless steel particles (approximately 90% by mass) suspended in a polymer binder, allowing the material to be printed in nearly an identical method to thermoplastics [8]. However, two stages of post-processing are required to produce a fully dense, metallic component. Immediately after printing, the component is referred to as a “green part” and looks visually similar to traditional FFF components since it is mostly composed of polymer binder. First the “green part” undergoes catalytic debinding, which removes a majority of the polymer binder, leaving behind a “brown part”. The remaining binder ensures the encased metallic powder remains the correct geometric shape. Finally, the “brown part” is sintered, causing the particles to combine into a fully dense steel part [9]. The result is a metallic component; however, this post-processing causes the parts to shrink anisotropically [10]. This process does not seek to replace traditional MBAM processes, but allows for the creation of metal components at a significantly reduced cost compared to traditional MBAM. While MEX will not likely be utilized to create structural components, there are many applications that will see higher stresses than plastics can withstand. Rapid prototyping and one-off production of components such as levers, instrument panels, or any class B1-B2 structure outlined in NASA’s “Standard for Additively Manufactured Spaceflight Hardware by Laser Powder Bed Fusion in Metals could be produced with MEX” [11].

A number of studies have been conducted to determine optimal process parameters and properties with Ultrafuse 316L. Thompson et al. [8] published one of the earliest overviews of the process, using a Prusa i3 Mk2 printer. Several studies have set out to determine optimal print parameters, varying nozzle temperature, infill strategy, build orientation, print speed, extrusion multiplier, line width, and layer height [12,13]. The effects of print parameters on shrinkage during processing [12,14–16], geometric accuracy [16], density [12,17,18], tension tests [8,13–15,18,19], optimization of post-processing [20], fatigue [21], hardness [14,18,22], and surface roughness [22] have been investigated, often comparing to samples produced from L-PBF [19,22], other MEX processes such as Desktop Metal and Markforged [21,22] or samples from conventionally manufactured 316L plate [8,14]. Typically industrial or commercial grade FFF printers have been utilized in previous research. Industrial printers such as the Apium P155 (\$10,000–\$25,000+) or commercial grade such as the Creatbot F430 [16], Lulzbot TAZ6 [20], Intamsys Funmat HT [19], Ultimaker S5 [12], Ultimaker 3 [13] (\$2000–\$10,000), or consumer grade such as Felix Tec 4 [15] and Prusa i3 [8,22] (\$1000–\$2000) have been utilized. At present, no studies have utilized any of the common hobbyist grade printers available for under \$500.

Previous research has established that printing specimens in the horizontal orientation provides the highest tensile strength [17]. Furthermore, it has been established that factors such as nozzle temperature have little effect on density [12]. The process has proved to produce 316L samples with tensile strengths similar to L-PBF or conventionally produced 316L but with a reduced yield strength [9,13] and approximately 2–5% porosity [8,12,14,17,22]. However, previous literature has highlighted that typical mechanical properties are reduced from those advertised by the manufacturer due to porosity [19]. Process-induced porosity is a significant issue for metal FFF, with pores naturally forming between parallel print lines during deposition and post-processing. The reported density from previous research varies, with reports of up to 95–98% dense parts [13,17], resulting from many different methods being utilized to calculate the volume/density/porosity. Previous research has utilized Archimedes principle [13], X-ray micro-computed tomography (micro CT) [17],

gas-pycnometry [12], and optical micrographs [8,17]. Damon et al. [17] correlated process-induced porosity to mechanical properties using micro CT and micrographs, concluding the formation of pores is strongly connected to build direction with elongated pore channels forming along parallel print paths and turning points between internal hatching and perimeters. Damon et al. [17] recommends further research focus on reduction of process-dependent porosity through optimization of extrusion parameters. These findings are further supported by Safka et al. [15] utilizing a 106% extrusion multiplier to increase tensile and yield strength; however, they did not report density or porosity. Developing an understanding of which extrusion parameters have the greatest potential to improve mechanical properties and mitigate porosity requires further investigation. Additionally, there is little understanding of how this may vary across multiple FFF machines and if process parameters are machine agnostic.

Previous research has only utilized one FFF printer within each respective study, often focusing on the effects of print parameters on density/shrinkage [12] or mechanical properties [13]. At present, the variation of optimal process parameters between FFF printers is not understood, since control software, slicing/print path, range of allowable parameters, and repeatability varies with each printer. There is little understanding of how equivalent print parameters vary between FFF printers. Few studies have compared multiple density measurement techniques, tension, and hardness testing across replicates within a single design of experiments.

To understand the variation of print parameters across multiple FFF printers, this study compares two FFF printers, by analyzing the effects of varying extrusion process parameters on density and mechanical properties with Ultrafuse 316L (BASF 3D Printing Solutions GmbH, Heidelberg, Germany). A Makerbot Method X, a commercial grade FFF printer is directly compared to a Creality Ender 3 V2, one of the lowest cost and most widely available hobbyist FFF printers. This study has three specific goals: evaluate if budget, hobbyist grade, FFF printers can utilize Ultrafuse 316L to produce metallic components for a total investment of approximately \$1000, explore the use of gas-pycnometry and optical micrographs to measure density, and evaluate the impact of extrusion process parameters on density and determine if they are machine agnostic.

2. Materials and Methods

This study utilized BASF UltraFuse 316L metal 3D filament to produce tensile specimens on two different FFF printers, the Creality Ender 3 V2 and the Makerbot Method X. For direct comparison, tensile specimens were produced via L-PBF and machined from 316L plate. L-PBF samples were manufactured using 316L powder on a Renishaw AM400. Density, microhardness, and tensile response was evaluated for all of the produced specimens. The price breakdown for the two FFF printers used in this work, the Renishaw AM400, and the feedstock used in each machine is presented in Table 1.

Table 1. Cost comparison of the machines and 316L feedstock materials utilized in this study (in USD).

Process	Machine	Approximate Cost	Approximate Feedstock Cost/kg
FFF	Creality Ender 3 v2	\$250	\$150 (filament)
	Makerbot Method X	\$5000	
L-PBF	Renishaw AM400	>\$250,000	\$200 (powder)

2.1. Printed Geometry

To compare the performance of specimens produced from each machine, sub-sized tensile specimens were printed on each respective machine following ASTM E8 [23]. Computer-aided design (CAD) geometries of the ASTM E8 sub-sized tensile specimens were created using SolidWorks. The FFF produced specimens were scaled up by 19.82% in the X/Y axes and by 26.10% in the Z axis to compensate for the shrinkage caused by the debinding and sintering process as outlined by BASF [9]. The specimen dimensions, after post-processing,

are shown in Figure 1. The geometries were sliced using Ultimaker Cura for the Ender 3 V2 and Makerbot CloudPrint for the Method X. The Ender 3 V2 used a more traditional $-45^\circ, +45^\circ$ alternating infill strategy for even/odd layers throughout the build height. The Method X cloud print used a $-45^\circ/+45^\circ$ alternating infill for even/odd layers, but only for layers 1–7. For layer 0 and layers 8–14, a $90^\circ/0^\circ$ alternating infill strategy is utilized, highlighted in Figure 2. The choice of infill strategy and two contour perimeters was per manufacturer recommendation [9].

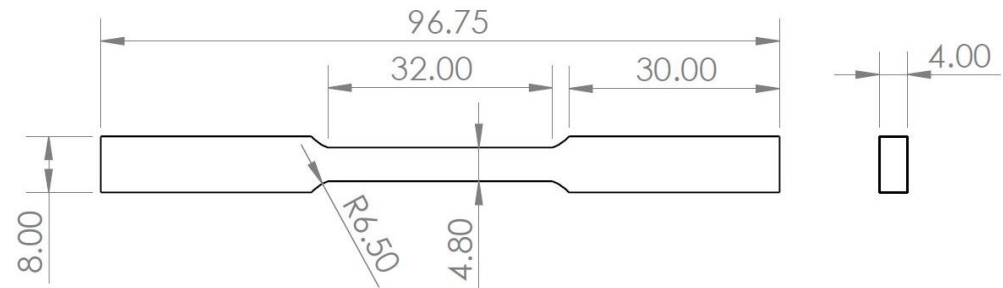


Figure 1. ASTM E8 subsized tensile specimen utilized throughout the study after post-processing, dimensions shown in mm.

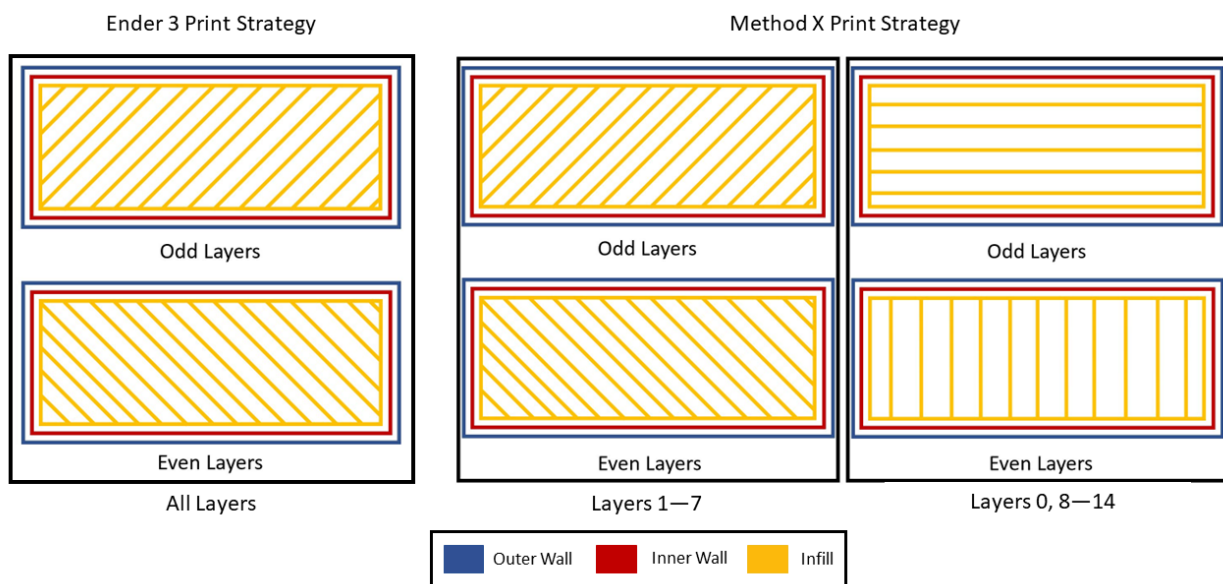


Figure 2. Build strategies for the Ender 3 V2 (Left) and Method X (Center & Right).

L-PBF samples were produced on a Renishaw AM400 [24], and the conventional 316L samples were waterjet from 316L plate for direct comparison. L-PBF samples were built in the vertical orientation with 316L stainless steel powder supplied by Renishaw, using the recommended process parameters. After printing, the L-PBF specimens were removed from the build plate using a vertical bandsaw. No additional post-processing was performed on the L-PBF or plate samples prior to tensile testing.

2.2. Design of Experiments

The original scope of this work was to conduct a full factorial DOE with the Ender 3 V2, varying the nozzle temperature, layer height, and print speed at three levels. Due to frequent print failure across extreme points of the DOE and conclusions of other studies [17], the design of experiments was pivoted to focus on extrusion parameters such as extrusion multiplier, line width, and layer height. Previous research suggests a combination of these parameters may lead to less process-induced porosity between print lines [17]. The two-level, three factor, factorial DOE with these parameters is highlighted in Table 2.

Table 2. 3-Factor, 2-Level design of experiments for Ender 3 V2 and Method X. Additional samples were printed at the Makerbot supplied parameters for Ultrafuse 316L for comparison.

Level	Line Width (mm)	Layer Height (mm)	Extrusion Multiplier (%)
1	0.3	0.1	100
2	0.5	0.25	120
Method X default	0.4	0.152	100

The ranges for these parameters were informed from recommendations of the manufacturer and the aforementioned DOE. The nozzle temperature was set to 240 °C, and the bed temperature was set to 100 °C with no fan cooling. The Ender 3 V2 was left in the stock configuration with the only modification being a hardened 0.4 mm nozzle at the recommendation of the manufacturer [9] and a custom printer enclosure [25]. Samples followed a standard naming convention with the FFF machine, level, and parameters in a EXXX format. Here the first number corresponds to the layer height, the second line width, and the third extrusion multiplier. For example, an Ender print at the lowest levels would be E111, and the highest E222.

The use of a MakerBot Method X allowed a commercial grade printer to be evaluated over the same range of parameters, and ultimately compared to a budget hobbyist grade FFF printer. Furthermore, the Method X natively supported the use of Ultrafuse 316L and was used in its stock configuration other than the addition of the MakerBot LABS experimental extruder with a 0.4 mm nozzle. The process parameters supplied with the MakerBot were also evaluated for comparison, as shown in Table 2. Print chamber heating on the Method X was utilized for each print at 100 °C per MakerBot recommendation, otherwise print parameters were consistent between FFF printers. Before starting a print on each machine, DimaFix, a water-soluble adhesive, was applied to the print bed to improve bed adhesion following recommendation from BASF [9].

During fabrication, there was difficulty printing process parameter combinations with two of the three parameters at the low settings. For example, E112, E121, E211 failed to print. However, parameter combinations with two parameters set to the high level such as E221, E122, and E212 all printed without issue. Additionally, prints at the maximum levels (E222) failed to print, but prints at the lowest levels (E111) printed successfully. Failed prints were determined by visual inspection of abnormal layer thickness, inconsistent bed adhesion, and loose material as depicted in Figure 3. These failures resulted in delamination shown in Figure 3c. Any as-printed samples with visible warpage, under extrusion/inter-layer de-bonding or parts that were bent, gouged, cracked, or separated from the build plate were considered failed prints. As a result, only four of the eight parameter combinations in the DOE could be evaluated on the Ender 3 V2, shown in Table 3.

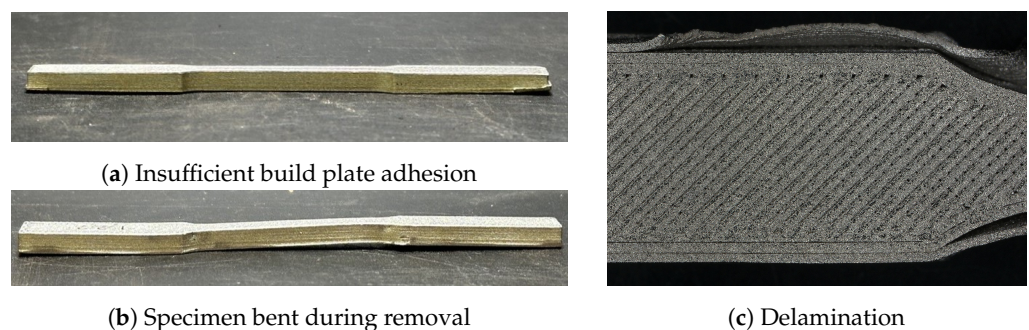


Figure 3. Post-processed print failures, highlighting print warpage (a), specimen damaged when removing from build plate (b), and resultant delamination of contours from infill (c).

Table 3. Successful print parameter combinations for Ender 3 V2 and Method X printers from the design of experiments that were analyzed in this study.

Specimen	Printer	Line Width (mm)	Layer Height (mm)	Extrusion Multiplier (%)
E111	Ender 3 v2	0.3	0.1	100
E221	Ender 3 v2	0.5	0.25	100
E122	Ender 3 v2	0.5	0.1	120
E212	Ender 3 v2	0.3	0.25	120
M111	Method X	0.3	0.1	100
M221	Method X	0.5	0.25	100
MBDS	Method X	0.4	0.152	100
MBDS1x1	Method X	0.4	0.152	100

Print failures also occurred with the Makerbot Method X, at similar process parameter combinations to the Ender 3 V2 resulting in the DOE being down-selected to M111, M221, M122 and M212 for direct comparison. Unfortunately, any prints utilizing the higher extrusion multiplier of 120% on the Method X resulted in failure. Furthermore, the increased extrusion rate caused sufficient material build up to damage a Makerbot LABS experimental extruder, and Makerbot has since advised against increasing the extrusion multiplier past 110%. Following this, only M111 and M221 were built on the Method X for direct comparison to E111 and E221. However, the recommended print parameters from MakerBot were evaluated for two cases. With the Ender 3 V2 utilizing Ultimaker Cura for build file preparation, and the Method X using Makerbot CloudPrint, limitations in each of the respective softwares resulted in the Ender 3 V2 samples being produced sequentially (part 1 fully built, followed by part 2, etc.), while all four Makerbot samples were built layer-wise. To compare these printing strategies, the default settings (MBDS) were used to produce 4 samples at a time, and to print a single sample at a time (MBDS1x1) as shown in Table 3.

2.3. Sample Processing

The as-printed FFF specimens, in their “green-part” state, were prepared for the sintering process by removing surface defects using 220 grit sandpaper per manufacturer recommendations [10]. Post-processing, consisting of catalytic debinding and sintering was outsourced and performed by DSC Technologies, LLC through a standard Ultrafuse processing ticket available through MatterHackers. The “green part” first undergoes catalytic debinding, leaving a “brown part” with enough polymer binder to maintain geometric accuracy. The “brown part” is then sintered, where the part is heated 5 °C/min from room temperature to 600 °C for one hour, then heated to 1380 °C for three hours before furnace cooling. Following processing, the samples are packaged and returned as a 316 L stainless steel part.

2.4. Material Characterization

Due to the variety of methods used to measure density in previous research, this study employed two methods to quantify internal defects and compared them. The first method involved using gas pycnometry to measure part density, and the second method was using optical micrographs (OM) to measure the OM density of the cross-section. Gas pycnometry measurements were taken using an Anton Paar Ultrapyc 5000 (Anton Paar GmbH, Graz, Austria). The default measurement configuration was utilized, where five density measurements are recorded and averaged for each sample. Density samples were extracted from the grip section using a diamond saw and were weighed using a Sartorius Secura 124 (Sartorius Lab Instruments GmbH & Co. KG, Goettingen, Germany) analytical balance.

To obtain the OM density, cross-sections of the gauge section were hot mounted with PolyFast, following standard metallographic preparation. Samples were ground on Silicon Carbide (SiC) (70–15 µm), before coarse polishing with Struers DiaPro (9 µm) and

DiaPro (3 μm) suspension. Fine polishing utilized Struers OP-U (0.04 μm) oxide polishing suspension. Optical micrographs were obtained with a Keyence VHX-7000 (Keyence Corporation, Higashi-Nakajima, Japan) and processed in ImageJ (version 1.54f) [26]. Default thresholding in ImageJ (version 1.54f) was performed on 8 bit images to calculate the porosity area of each samples cross-section. The size and circularity for particle analysis was adjusted to remove non-porosity noise. This was repeated for three samples ($n = 3$) of each parameter combination. Circularity was defined as 4π (area/perimeter²), where more elongated pores having a value approaching zero. A JEOL 6500F (JEOL Ltd., Tokyo, Japan) field emission scanning electron microscope (SEM) was used to take secondary electron images of the fractured tensile specimens for one Makerbot-produced specimen and one Ender-produced specimen.

Vickers hardness testing was performed using a (Buehler, Bluff, IL, USA) microhardness indenter. Samples extracted for hardness testing were taken from the grip section. The extracted cross-sections were mounted, ground, and polished as previously outlined. A grid of indentations spanning the cross-sectional surface was created with an indent spacing of 0.5 mm and a distance to edge of 0.25 mm, resulting in approximately 40 indents per specimen. Following ASTM E92, indentations were created using a 500 gf load with a 10 s dwell time [27]. Hardness testing was repeated on three samples from each parameter set.

Tensile tests were conducted using an Instron 5882 (Instron Mechanical Testing Systems, Norwood, MA, USA) at a strain rate of 0.03/s, following ASTM E8 [23]. An extensometer was used to measure strain during the elastic regime, and after yield was reached, the extensometer was removed and strain to failure was calculated using crosshead displacement. A total of five tests were performed for each FFF parameter set (excluding E212), the L-PBF produced samples, and 316L plate samples.

3. Results & Discussion

The measured density, relative density, and optical microscopy (OM) density of FFF and L-PBF specimens are presented in Table 4. Relative density and OM density is both presented relative to the published density of 316L stainless steel of 7.84 g/cm³ [21]. OM density was measured from micrographs of three specimens for each process parameter combination. The MBDS samples exhibited the highest OM density at 99.3% for specimens printed one-by-one and four at a time. However, M221 demonstrated a similar OM density of 99.1%. The Ender samples exhibited a maximum OM density of 95.9% for E212, and minimum of 80.8% for E221.

Table 4. Average density & standard deviation measured by gas-pycnometer and optical microscopy density ($n = 3$) of the FFF samples.

Specimen	Measured Density (g/cm ³)	Relative Density (%)	OM Density (%)
E111	7.8206 \pm 0.3012	99.8	89.0 \pm 0.88%
E221	7.9161 \pm 0.2424	101	80.8 \pm 2.59%
E122	7.7874 \pm 0.2212	99.3	94.7 \pm 0.53%
E212	7.7133 \pm 0.2113	98.4	95.9 \pm 0.80%
M111	7.6695 \pm 0.3595	97.8	97.7 \pm 1.19%
M221	7.7246 \pm 0.2319	98.5	99.1 \pm 0.13%
MBDS	7.7694 \pm 0.1982	99.1	99.3 \pm 0.29%
MBDS1x1	7.6902 \pm 0.1667	98.1	99.3 \pm 0.31%
L-PBF	7.8018 \pm 0.0783	99.5	99.5 \pm 0.31%

Method X samples demonstrated the highest OM density with little difference in mechanical strength between all parameter combinations. However, a difference in strength and porosity was present in the Ender samples. E122 and E212 performed the best with only a 7–10% reduction in strength as compared to the average Method X sample. E221 and E111 had a significant reduction in mechanical strength with the lowest OM density. The average ($n = 5$) mechanical response and the standard deviation is presented in Table 5. A

representative stress-strain curve is presented in Figure 4, where “S” denotes the sample shown on the plot.

Ender samples made with the 120% extrusion multiplier obtained comparable mechanical properties to previous research, but had a reduced yield strength of 135–142 MPa compared to previous values of 153–180 MPa in literature [13,14,19]. All of the Method X prints obtained comparable or improved properties to previous research. The Young’s modulus was comparable to the 151.3–185 GPa [13,14,17] and tensile strength was higher than the 465–498 MPa [13,14] reported in previous studies. Due to porosity, only three E212 (0.5 mm line width, 0.1 mm layer height, and 120% extrusion) samples were produced. Furthermore, large irregular pores in E111 meant hardness testing could not be performed. The most dense Ender sample, E212 and least dense, E221, when compared show the same trend of reduced strength and elongation as previous research [28].

Table 5. Average & standard deviation for mechanical response ($n = 5$) & Vickers hardness ($n = 3$) for successful print parameter combinations.

Specimen	Elastic Modulus (GPa)	Yield Strength (MPa)	UTS (MPa)	Hardness (HV0.5)
E111	131.2 ± 15.40	103.2 ± 21.41	271.5 ± 41.95	N/A
E221	121.4 ± 17.7	84.29 ± 9.21	306.04 ± 17.07	176.8 ± 50.87
E122	136.2 ± 12.75	134.8 ± 19.98	434.25 ± 33.58	176.2 ± 35.73
E212 *	176.3 ± 29.77	141.8 ± 10.29	466.2 ± 19.08	182.6 ± 37.96
M111	170.0 ± 17.31	153.8 ± 7.20	506.3 ± 2.79	179.1 ± 34.96
M221	179.7 ± 06.47	148.1 ± 5.80	505.3 ± 6.14	179.6 ± 33.49
MBDS	166.0 ± 19.04	158.2 ± 6.18	513.7 ± 2.77	181.0 ± 27.75
MBDS1x1	165.5 ± 18.56	154.3 ± 2.86	509.5 ± 1.21	188.4 ± 37.27
L-PBF	190.6 ± 07.69	395.38 ± 13.33	536.63 ± 9.39	220.9 ± 23.46
316L Plate	185.0 ± 11.09	302.54 ± 05.10	631.33 ± 2.85	193.7 ± 18.59

* Only collected mechanical properties for ($n = 3$); Hardness could not be obtained for E111 due to porosity.

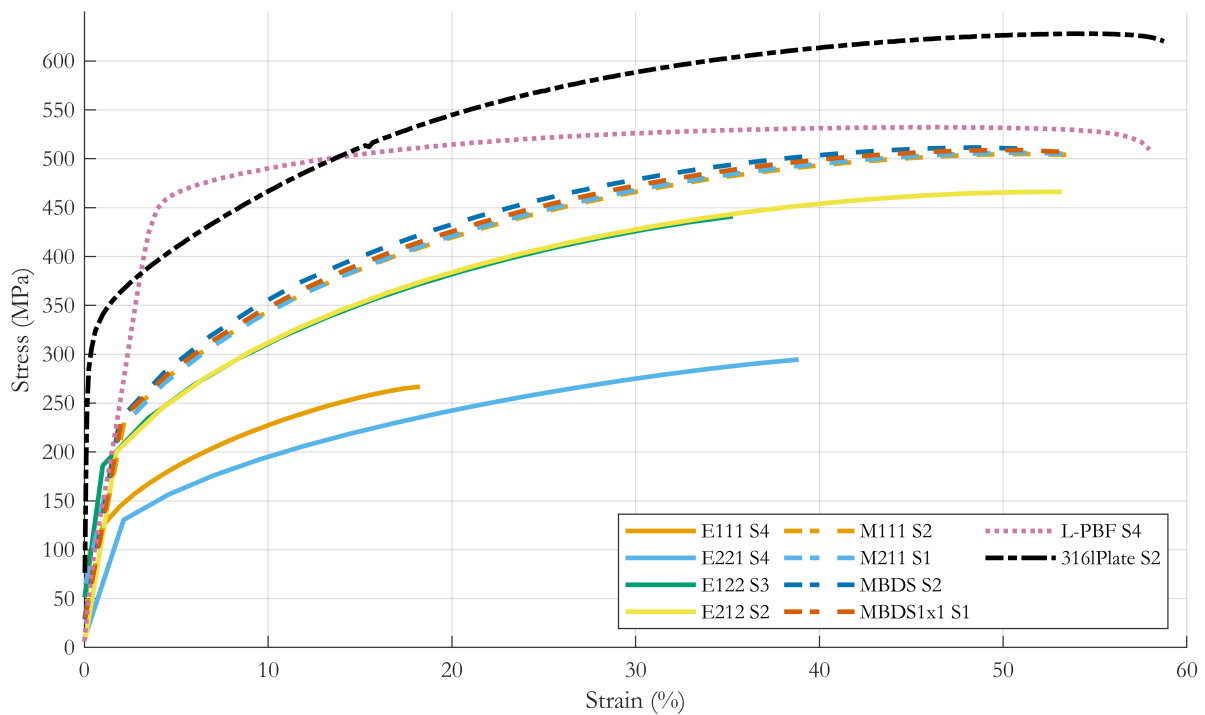


Figure 4. Engineering stress-strain plot for each process parameter combination, where “S” indicates the sample shown.

3.1. Gas Pycnometry vs. Optical Microscopy Density (%)

Since gas pycnometry measures enclosed volume, the reported density is of the solid components and only accounts for entrapped porosity, resulting in artificially high density values for these samples due to elongated, open pores. Optical microscopy can account for both open and closed porosity within the sample and produces density values more representative of the bulk component density when open pores are present. Even with an increased porosity, the Ender samples often had open pores forming along print lines, causing the artificial increase in measured density. The Method X and L-PBF samples often had closed pores, resulting in the more representative measured density, which correlates to the respective OM density. While gas-pycnometry can accurately measure density when closed pores are present, OM density or μCT should be utilized to accurately measure density when open pores are present. Examples of the process-induced porosity is highlighted in Figure 5.

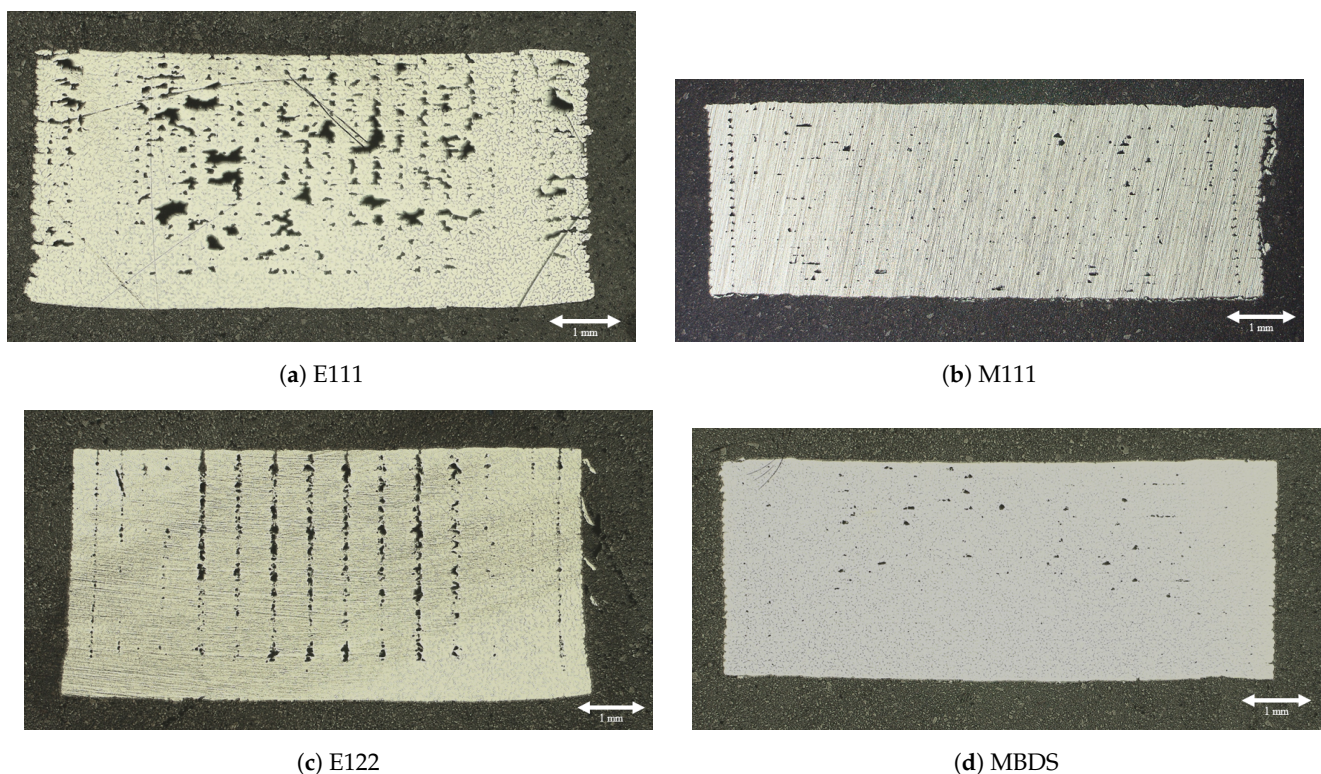


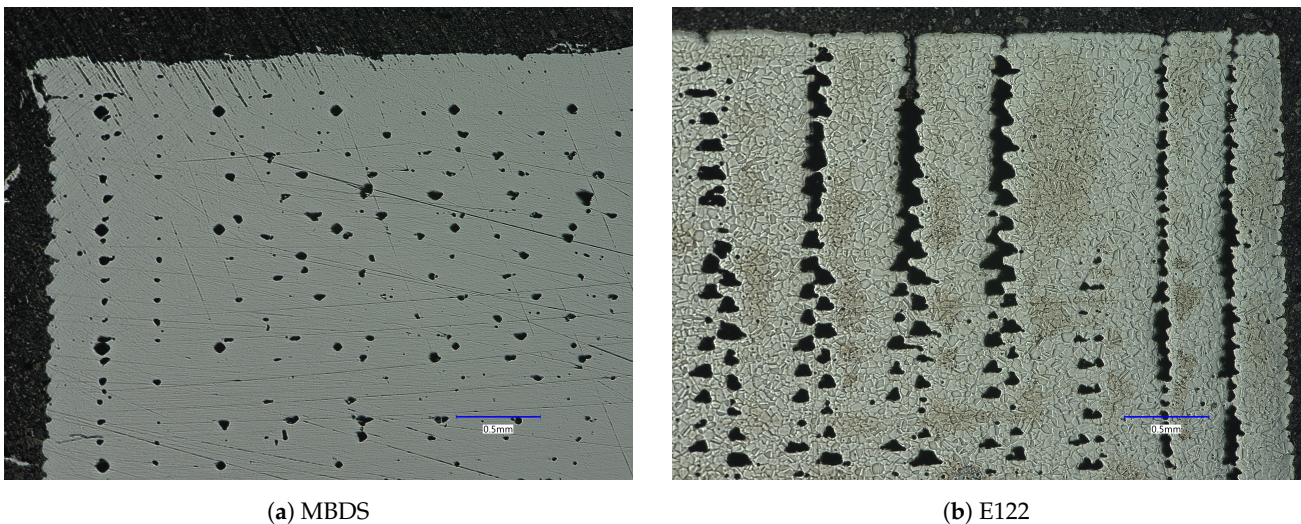
Figure 5. Optical Micrographs of cross-sections for Ender 3 V2 produced samples (a) E111 & (c) E122 and Method X produced samples (b) M111 & (d) MBDS.

3.2. Process-Induced Porosity

The distribution, shape, and size of pores varied with combinations of process parameters and between both FFF printers. At the lowest line width, layer height, and extrusion multiplier, porosity is the most exaggerated. E111 featured large irregularly shaped pores/voids (average pore size of 12 μm and circularity of 0.32), alongside small pores distributed throughout. Pores were much smaller and more regularly shaped in the M111 samples, with an average pore size of 1.5 μm and circularity of 0.53. However, both 111 samples show a trend of pores forming in the vertical direction, particularly around the exterior faces, and the interface of the two outer contours shown in Figure 5a,b.

In general, closed pores were present in Method X samples between print lines and layers throughout the infill regions. Porosity in Ender samples followed two trends: (a) homogeneous porosity across the infill region when the 100% extrusion multiplier was used (Figure 5a,b) and the formation of pores along the vertical direction when the 120% extrusion multiplier is used, which is exaggerated at the contour-infill interface (Figure 5c).

The spacing between the vertical pores within the infill region of sample E122 (0.57 mm) is slightly larger than the target line width of 0.5 mm for these parts. The differences in closed vs. open porosity between the two FFF printers (Figure 6) suggest the influence of uncontrolled process variables. Examples could include differences in machine architecture such as filament feed mechanism or chamber temperature control. Though these factors were not accounted for in this study, they are potential contributors to the discrepancy between specimens made on two different systems while the primary printing parameters were held constant.



(a) MBDS

(b) E122

Figure 6. Pore formation in the build direction in the Method X MBDS samples (a), and Ender 3 V2 E122 samples (b).

The aforementioned differences in distribution, shape, and amount of porosity impacted the mechanical response. All Method X specimens had an OM density of over 97%, and the Ender 3 V2 specimens had a maximum OM density of 96%. The small isolated pores in Method X samples did not greatly reduce the elastic modulus, but are likely responsible for the reduction in yield strength without greatly impacting tensile strength. The large irregular pores in the E111 specimens highlight the other extreme of this trend, where the elastic modulus is decreased due to reduction in effective cross-area, and the yield and tensile strengths were reduced due to stress concentrations around larger voids/pores.

3.3. Differences in FFF Printers

As expected, there are a variety of differences between the Method X and Ender 3 V2. The Method X has an automated bed leveling system, with built in calibration to maintain reproduce-ability. The Ender 3 V2 has no such system, requiring the print bed to be leveled by hand. Furthermore, it is up to the user to maintain/calibrate the printer and is susceptible to changes over time. Additionally, the build chamber of the Ender 3 V2 has no heating aside from the print bed to maintain the temperature within the printers enclosure, while the Method X has a heated bed and build chamber. The Ender 3 V2 uses a bowden tube style extruder, as opposed to the direct drive extruder used on the Makerbot Method X. While base capabilities of both systems are similar, the additional features of the Method X reduce human-factor induced variability and provide a larger processability space.

It is worth noting, other than an upgraded nozzle, the Ender 3 V2 was completely stock, as it came out of the box. This was done to evaluate the performance of this FFF printer off the shelf, as it is widely utilized. There are many aftermarket components and modifications that may improve the repeatability and performance of the Ender 3 V2 when printing with Ultrafuse 316L (BASF 3D Printing Solutions GmbH, Heidelberg, Germany). Examples of modifications to mitigate environmental effects and improve print consistency could include an upgraded hot-end, a heated build chamber, and utilizing the auto-bed

leveling system. Despite best efforts of setup and maintenance, the Ender does not have the repeatability of commercial grade FFF printers in its stock configuration.

3.4. Specimen Failure

All samples exhibited ductile tensile behavior. The fracture surfaces in Figure 7 show ductile fracture, although the fracture surface is rather unique for the Ender sample in Figure 7b. Typical necking was evident in the more dense samples, but the less dense samples exhibited more elongation of the infill “fibers” as opposed to the bulk structure. Failure of the more porous samples occurred along planes perpendicular to the infill paths producing a faceted surface (Figure 7b) or a 45° plane (Figure 8b). Good fusion of the contour pass to infill passes as shown in Figure 7b led to improved mechanical response.

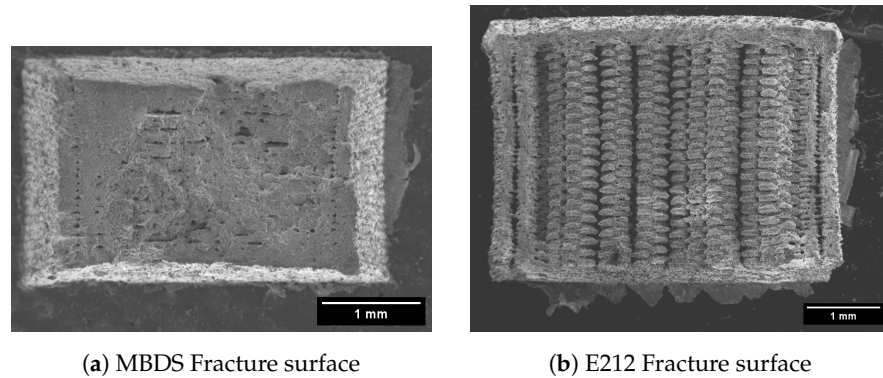


Figure 7. SEM image comparison of representative tensile fracture surfaces between Makerbot at 17× (a) and Ender produced samples at 16× (b).

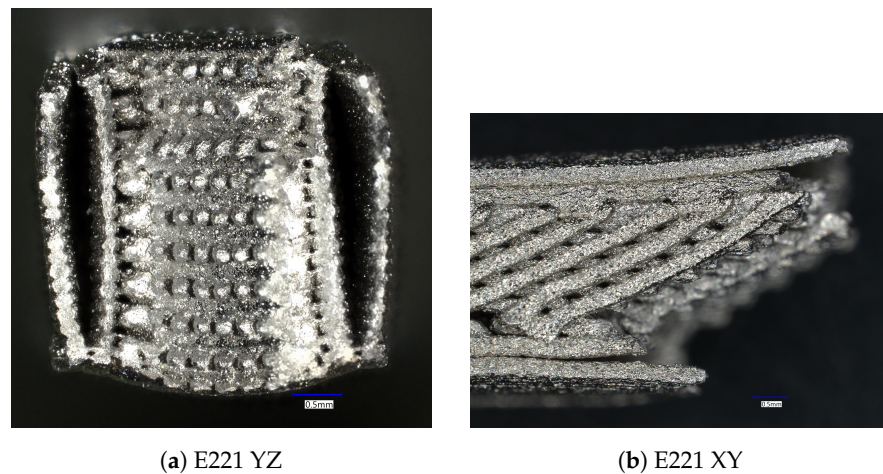


Figure 8. Optical image at 50× of failure in E221 samples, with “non-bulk” behavior at the fracture surface (a) and side profile (b).

Several samples showed delamination of the infill from the contour paths as in Figure 8a. The more porous samples typically failed along one of the 45° infill paths. Both Figure 8a,b show that only a portion of the infill was carrying load, leading to a higher stress on the remaining sections and reducing the bulk strength of the component. The larger, regularly patterned pores with continuous infill lines of E221 showed poorer mechanical strength but higher ductility than E111 which had more seemingly random porosity.

3.5. Effects of Print Strategy

As previously stated, the Ender 3 V2 and Method X utilized different software for slicing. Both machines used 2 outer contours per recommendation of previous research, and different patterns for alternating infill strategy throughout the build height as previously highlighted in Figure 2 [9,17]. The increase in porosity levels in the upper half of the

MBDS specimen (Figure 5d) suggests that infill porosity is dependent on printing strategy. However, the consistent lack of adhesion at the contour-infill interface throughout the build height suggests this defect pattern is extrusion parameter dependent. The differences in porosity throughout the build height between FFF printers suggest further research is needed.

3.6. L-PBF/Plate Comparison

The L-PBF produced samples resulted in the highest elastic modulus, yield strength, and hardness of all tested samples. L-PBF showed an increase of 11%, 62%, and 5% for the elastic modulus, yield strength, and tensile strength compared to the average Method X response. In previous research, a Renishaw AM400 was compared to MEX samples in the same build configuration (and powder supplier) and showed a 32% reduced elastic modulus, but a 12% increase in yield strength and a 6% increase in tensile strength [19], highlighting the variability present in L-PBF and environmental factors. However, the 316L plate specimens featured the highest ultimate tensile strength at 631 MPa. The hardening behavior of the FFF samples follows a similar trend to that of the 316L plate samples. The produced L-PBF samples showed minimal hardening, consistent with other vertically printed L-PBF 316L components [19,29]. Makerbot and Ender FFF parts showed similar yield strengths with approximately 50% and 40% reduction of yield strength compared to plate and L-PBF samples, respectively.

3.7. Future Work

A more accurate specimen density could be achieved by performing micro CT as done in [17]. This would reduce the effects of irregularities such as open pores during gas pycnometry measurements or location dependence of optical micrographs. Furthermore, micro CT could provide additional insight into the subtle differences between MBDS and MBDS1x1. While there was an insignificant difference in mechanical response of MBDS and MBDS1x1, further testing would need to be performed to fully conclude that there is no significant difference between printing samples on a per-part vs per-layer basis with regards to part density and strength.

Future research should investigate the effects of print strategy on process-induced porosity, and consider the evaluation of printing parameters not within the scope of this work (i.e., layer rotation angle, number of perimeters, perimeter overlap, and further investigation into extrusion parameters). Additionally, a higher sample size of OM density measurements taken from different regions and cross-sectional planes of the sample may help to elucidate some of the unique porosity phenomena occurring in these samples.

4. Conclusions

This research evaluated the use of two FFF printers, the Makerbot Method X and the Creality Ender 3 V2, to print tensile specimens using Ultrafuse 316L filament. Layer height, line width, and extrusion multiplier were varied for each printer, and the resulting tensile response, microhardness, and density were compared. The resulting mechanical properties were comparable to those published in literature for components printed with Ultrafuse 316L filament. The Method X produced 99% dense 316L specimens using the default print settings, and all successful print parameter combinations gave comparable or improved mechanical results compared to previous research. The Ender samples with an increased extrusion multiplier from the default parameters showed comparable strength to the Makerbot produced samples and literature data, but had a reduced OM density of approximately 95%. Porosity reduced the mechanical strength of the Ender samples, shown by process parameter combinations with an extrusion multiplier of 100%.

Additionally, the aforementioned FFF parameter combinations produced comparable elastic modulus, and slightly reduced tensile strengths compared to the L-PBF samples. Both L-PBF and FFF samples showed reduced tensile strengths compared to the plate material. FFF produced samples showed a reduction in yield strength, approximately

50% of 316L plate and 40% of L-PBF produced samples for both the Makerbot and Ender produced parts. This work supports the claim that FFF metal printing is a viable, low-cost option for lower strength requirement metal components. Comparing between FFF printers, the optimal settings for the Ender 3 V2 showed only a 7–8% reduction in yield and tensile strength compared to the average Method X sample. This is substantial, considering the Ender 3 v2 costs 95% less than the Method X. Accordingly, this work demonstrated that users are not limited to printing this material on higher-end FFF printers, but with the right settings, metal parts can be produced using a low-cost, hobby-grade printer with minimal modifications or up-front costs.

Author Contributions: Conceptualization, J.L.B., F.M.B. and M.W.P.; Methodology, J.L.B., B.J.S., K.L. and F.M.B.; Investigation, K.L., B.J.S., F.M.B. and J.L.B.; Writing—original draft preparation J.L.B., K.L. and B.J.S.; Writing—Review and Editing, J.L.B., F.M.B., B.J.S. and M.W.P.; Visualization, J.L.B.; Funding Acquisition, M.W.P. All authors have read and agreed to the published version of the manuscript.

Funding: This research was supported by funding from the Office of Research and Economic Development (ORED) at Mississippi State University (MSU) and the Bagley College of Engineering (BCoE) at MSU.

Data Availability Statement: The raw data supporting the conclusions of this article will be made available by the authors on request.

Acknowledgments: The authors would like to thank Mississippi State University (MSU) for fostering an environment that supports undergraduate research. MWP would like to thank the Center for Advanced Vehicular Systems (CAVS) for support/access to the gas pycnometer and the Institute for Imaging and Analytical Technologies (I2AT) for assistance using the Keyence microscope. The authors would also like to thank Haley Peterson for assistance performing mechanical testing.

Conflicts of Interest: The authors declare no conflicts of interest.

References

1. Kuznetsov, V.; Solonin, A.; Urzhumtsev, O.; Schilling, R.; Tavitov, A. Strength of PLA Components Fabricated with Fused Deposition Technology Using a Desktop 3D Printer as a Function of Geometrical Parameters of the Process. *Polymers* **2018**, *10*, 313. [[CrossRef](#)]
2. Arbogast, A.; Nycz, A.; Noakes, M.W.; Wang, P.; Masuo, C.; Vaughan, J.; Love, L.; Lind, R.; Carter, W.; Meyer, L.; et al. Strategies for a scalable multi-robot large scale wire arc additive manufacturing system. *Addit. Manuf. Lett.* **2024**, *8*, 100183. [[CrossRef](#)]
3. Armstrong, M.; Mehrabi, H.; Naveed, N. An overview of modern metal additive manufacturing technology. *J. Manuf. Process.* **2022**, *84*, 1001–1029. [[CrossRef](#)]
4. Petersen, H.E.; Sampson, B.J.; Failla, D.P., Jr.; Priddy, M.W.; McClelland, Z.B. The Variation of Mechanical Properties of M300 Maraging Steel Manufactured with Varying Process Parameters in Laser Powder Bed Fusion. In Proceedings of the 34rd Annual International Solid Freeform Fabrication Symposium 2023, Austin, TX, USA, 14–16 August 2023.
5. Kotadia, H.; Gibbons, G.; Das, A.; Howes, P. A review of Laser Powder Bed Fusion Additive Manufacturing of aluminium alloys: Microstructure and properties. *Addit. Manuf.* **2021**, *46*, 102155. [[CrossRef](#)]
6. Sampson, B.J.; Morgan-Barnes, C.; Stokes, R.; Doude, H.; Priddy, M.W. Investigating the Relationship between In-Process Quality Metrics and Mechanical Response in the L-PBF Process. In Proceedings of the 33rd Annual International Solid Freeform Fabrication Symposium 2022, Austin, TX, USA, 25–27 July 2022. [[CrossRef](#)]
7. Nurhudan, A.I.; Supriadi, S.; Whulanza, Y.; Saragih, A.S. Additive manufacturing of metallic based on extrusion process: A review. *J. Manuf. Process.* **2021**, *66*, 228–237. [[CrossRef](#)]
8. Thompson, Y.; Gonzalez-Gutierrez, J.; Kukla, C.; Felfer, P. Fused filament fabrication, debinding and sintering as a low cost additive manufacturing method of 316L stainless steel. *Addit. Manuf.* **2019**, *30*, 100861. [[CrossRef](#)]
9. BASF. *Ultrafuse Metal Filaments—User Guidelines for 3D Printing Metal Parts*; BASF 3D Printing Solutions GmbH: Heidelberg, Germany, 2021.
10. BASF. *Ultrafuse 316l Technical Data Sheet*; BASF 3D Printing Solutions GmbH: Heidelberg, Germany, 2022.
11. Aeronautics, N.; Standard, S.A. *Standard for Additively Manufactured Spaceflight Hardware by Laser Powder Bed Fusion in Metals*; Technical Report; MSFC—Marshall Space Flight Center: Huntsville, AL, USA, 2023.
12. Quarto, M.; Carminati, M.; D’Urso, G. Density and shrinkage evaluation of AISI 316L parts printed via FDM process. *Mater. Manuf. Process.* **2021**, *36*, 1535–1543. [[CrossRef](#)]

13. Caminero, M.A.; Romero, A.; Chacon, J.M.; Nunez, P.J.; Garcia-Plaza, E.; Rodriguez, G.P. Additive manufacturing of 316L stainless-steel structures using fused filament fabrication technology: Mechanical and geometric properties. *Rapid Prototyp. J.* **2021**, *27*, 583–591. [[CrossRef](#)]
14. Gong, H.; Crater, C.; Ordonez, A.; Ward, C.; Waller, M.; Ginn, C. Material Properties and Shrinkage of 3D Printing Parts using Ultrafuse Stainless Steel 316LX Filament. *MATEC Web Conf.* **2018**, *249*, 01001. [[CrossRef](#)]
15. Safka, J.; Ackermann, M.; Machacek, J.; Seidl, M.; Vele, F.; Truxova, V. Fabrication Process and Basic Material Properties of the Basf Ultrafuse 316Lx Material. *MM Sci. J.* **2020**, *2020*, 4216–4222. [[CrossRef](#)]
16. Pellegrini, A.; Guerra, M.G.; Lavecchia, F. Shrinkage evaluation and geometric accuracy assessment on 17–4 PH samples made by material extrusion additive manufacturing. *J. Manuf. Process.* **2024**, *109*, 394–406. [[CrossRef](#)]
17. Damon, J.; Dietrich, S.; Gorantla, S.; Popp, U.; Okolo, B.; Schulze, V. Process porosity and mechanical performance of fused filament fabricated 316L stainless steel. *Rapid Prototyp. J.* **2019**, *25*, 1319–1327. [[CrossRef](#)]
18. Khanafer, K.; Park, J.S.; Eltaggaz, A.; Aboelkassem, Y. Investigation of the Mechanical Characteristics of Metal 3D Printing at Different Build Orientation and Directions. *J. Eng. Mater. Technol.* **2024**, *146*, 031001. [[CrossRef](#)]
19. Kedziora, S.; Decker, T.; Museyibov, E.; Morbach, J.; Hohmann, S.; Huwer, A.; Wahl, M. Strength Properties of 316L and 17–4 PH Stainless Steel Produced with Additive Manufacturing. *Materials* **2022**, *15*, 6278. [[CrossRef](#)]
20. Wang, F.; You, S.; Jiang, D.; Yuan, X.; Fu, R.; Ning, F. Microstructure evolution, phase formation, corrosion, and mechanical properties of stainless steel fabricated by extrusion-based sintering-assisted additive manufacturing. *Addit. Manuf.* **2023**, *75*, 103746. [[CrossRef](#)]
21. Suwanpreecha, C.; Songkuea, S.; Linjee, S.; Muengto, S.; Bumrungpon, M.; Manonukul, A. Tensile and axial fatigue properties of AISI 316 L stainless steel fabricated by materials extrusion additive manufacturing. *Mater. Today Commun.* **2023**, *35*, 105667. [[CrossRef](#)]
22. Kluczyński, J.; Jasik, K.; Łuszczek, J.; Sarzyński, B.; Grzelak, K.; Dražan, T.; Joska, Z.; Szachogluchowicz, I.; Płatek, P.; Małek, M. A Comparative Investigation of Properties of Metallic Parts Additively Manufactured through MEX and PBF-LB/M Technologies. *Materials* **2023**, *16*, 5200. [[CrossRef](#)]
23. ASTM-International. *ASTM E8/E8M, Standard Test Methods for Tension Testing of Metallic Materials*; Technical Report; ASTM International: West Conshohocken, PA, USA, 2021.
24. Stokes, R.M.; Yadollahi, A.; Priddy, M.W.; Bian, L.; Hammond, V.H.; Doude, H.R. Effects of Build Interruption and Restart Procedure on Microstructure and Mechanical Properties of Laser Powder Bed Fusion Al-Si-10 Mg. *J. Mater. Eng. Perform.* **2023**, *32*, 1576–1588. [[CrossRef](#)]
25. Cisardom. Original Prusa i3 MK3 ENCLOSURE—Ikea Lack Table—Prusa Research. 2018. Available online: <https://www.thingiverse.com/thing:2864118> (accessed on 8 March 2021).
26. Schindelin, J.; Arganda-Carreras, I.; Frise, E.; Kaynig, V.; Longair, M.; Pietzsch, T.; Preibisch, S.; Rueden, C.; Saalfeld, S.; Schmid, B.; et al. Fiji: An open-source platform for biological-image analysis. *Nat. Methods* **2012**, *9*, 676–682. [[CrossRef](#)]
27. E28 Committee. *Test Methods for Vickers Hardness and Knoop Hardness of Metallic Materials*; Technical Report; ASTM International: West Conshohocken, PA, USA, 2023. [[CrossRef](#)]
28. Atatreh, S.; Alyammahi, M.S.; Vasilyan, H.; Alkindi, T.; Susantyoko, R.A. Evaluation of the infill design on the tensile properties of metal parts produced by fused filament fabrication. *Results Eng.* **2023**, *17*, 100954. [[CrossRef](#)]
29. Afkhami, S.; Dabiri, M.; Piili, H.; Björk, T. Effects of manufacturing parameters and mechanical post-processing on stainless steel 316L processed by laser powder bed fusion. *Mater. Sci. Eng. A* **2021**, *802*, 140660. [[CrossRef](#)]

Disclaimer/Publisher’s Note: The statements, opinions and data contained in all publications are solely those of the individual author(s) and contributor(s) and not of MDPI and/or the editor(s). MDPI and/or the editor(s) disclaim responsibility for any injury to people or property resulting from any ideas, methods, instructions or products referred to in the content.